processes

MDPI

Article

Sustainable Production of Porous Activated Carbon from Hydrothermally Carbonized Jamoya Fruit Seeds and Its Potential for Adsorbing the Azo Dye Carmoisine B

Shubham Chaudhary [1,2], Monika Chaudhary [3], Vaishali Tyagi [2], Shivangi Chaubey [2], Suhas [2,*], Vikas Gupta [1], Isabel Pestana da Paixão Cansado [4,5,*] and Jahangeer Ahmed [6]

1 Department of Chemistry, Motherhood University, Roorkee 247661, India; shubhamchaudhary89@yahoo.com (S.C.); drvikasgupta2510@gmail.com (V.G.)
2 Department of Chemistry, Gurukula Kangri (Deemed to be University), Haridwar 249404, India; tyagivaish1@gmail.com (V.T.); shivangichaubey34@gmail.com (S.C.)
3 Department of Chemistry, Hariom Saraswati P.G. College, Dhanauri, Haridwar 247667, India; monikachoudry@gmail.com
4 MED—Mediterranean Institute for Agriculture, Environment and Development & Change—Global Change and Sustainability Institute, Universidade de Évora, Pólo da Mitra, Apartado 94, 7006-554 Évora, Portugal
5 Department of Chemistry and Biochemistry and School of Science and Technology, University of Évora, Rua Romão Ramalho, nº 59, 7000-671 Évora, Portugal
6 Department of Chemistry, College of Science, King Saud University, P.O. Box 2455, Riyadh 11451, Saudi Arabia; jahmed@ksu.edu.sa
* Correspondence: suhasnatyan@yahoo.com (S.); ippc@uevora.pt (I.P.d.P.C.)

Abstract: Porous carbon materials can serve as effective and versatile adsorbents in water pollution management. This study presents a cost-effective and environmentally friendly method to produce porous carbon materials (JFS-PC) by exploiting Jamoya fruit seeds (JFS) as a precursor using a hydrothermal carbonization (HTC) process. HTC is a thermochemical process for the conversion of high moisture content biomass into carbon-rich materials. The process is performed in a temperature range of 180–250 °C during which the biomass is submerged in water and heated in a sealed environment under autogenous pressure. The adsorbents obtained were explored using different techniques viz. XRD, FTIR, FE-SEM, and surface area analyses to evaluate their characteristics that are beneficial for the adsorption process. Surface area analysis revealed that the developed activated carbon exhibits appreciable surface area (440.8 m^2g^{-1}), with a mean pore diameter of 3.97 nm. Activated carbon was successfully tested on the removal of an azo dye, Carmoisine B (CB), from water systems. Isothermal and kinetic evaluation demonstrated that the dye adsorption agrees well with the Langmuir (R^2 = 0.993) and pseudo-second-order (R^2 = 0.998) kinetics models. The experiments were designed to investigate the influence of adsorbate concentration (1×10^{-4} and 2×10^{-4} mol L^{-1}), collision time (5–300 min), pH (2–12) of the solution, and temperature (25–45 °C) on the adsorption of the selected dye. The results revealed that pH influences the adsorption capacity of CB and showed maximum adsorption between pH 2 and 5. Experimentally, the CB isotherms showed maximum adsorption capacities of 169.0 mg g^{-1}, at 45 °C. Mechanisms indicate that the surface charge of the adsorbent, and structures of the adsorbate play key roles in adsorption. Thermodynamic parameters revealed an endothermic and a physisorption process supported by Van't Hoff calculations. The study indicates that the developed porous carbon (JFS-PC) can be successfully used for the removal of CB from water systems. It also highlights the use of an inexpensive and renewable precursor for the development of porous carbon materials.

Keywords: hydrothermal carbonization; hydrochar; porous carbon; adsorption; Carmoisine B

Academic Editor: Monika Wawrzkiewicz

Received: 10 December 2024
Revised: 25 January 2025
Accepted: 28 January 2025
Published: 31 January 2025

Citation: Chaudhary, S.; Chaudhary, M.; Tyagi, V.; Chaubey, S.; Suhas; Gupta, V.; Pestana da Paixão Cansado, I.; Ahmed, J. Sustainable Production of Porous Activated Carbon from Hydrothermally Carbonized Jamoya Fruit Seeds and Its Potential for Adsorbing the Azo Dye Carmoisine B. *Processes* **2025**, *13*, 385. https://doi.org/10.3390/pr13020385

1. Introduction

The agricultural, industrial, pharmaceutical, and building sectors are actively involved in the use of a huge amount of natural resources and consequently produce a large amount of biomass waste that impacts the environment. Inadequate management of biomass waste has attracted the attention of the scientific community to develop new strategies for managing it, in order to promote sustainability [1]. The valorization of biomass waste resources by converting them into porous carbon materials has emerged as an effective approach for their application in water treatment in the recent years [2–4].

Biomass including agricultural waste [5], apricot stones [6], eucalyptus barks [7], almond shells [8], bamboo sawdust [9], Tectona grandis sawdust, stubble, fibers from the Adansonia digitata L. tree, and bamboo flower [10], were used in numerous studies for the production of porous carbons, mainly activated carbons (ACs). The hydrothermal conversion of biomass waste into porous materials has become the research focus in recent years due to its energy efficiency, usage of low temperature, and it not needing pre-drying features as compared to the pyrolysis, gasification, and torrefaction techniques. Moreover, water is used as a solvent during HTC which diminishes the use of hazardous chemicals and is thereby termed as an environmentally friendly process. No hazardous emissions of gasses are produced during the HTC process, which represents a benefit over other methods. Additionally, the carbons produced via the hydrothermal route are rich in carboxylic, ketonic, and phenolic groups [10–12] which are useful for adsorption applications.

Azo dyes have been widely exploited in various industrial processes for coloring leather, textiles, and as food colorants [13–15]. Due to the low production cost of azo dyes, they are extensively used and their production reached 8.8×10^3 metric tons in 2023, and is anticipated to reach 11×10^3 metric tons by 2029 [16]. Among these dyes, Carmoisine B (CB), anionic in nature, is widely used for dyeing purposes and as a food colorant [17]. However, CB has been reported to cause neurological, allergic, carcinogenic, and hyperactivity disorders in humans [13] and therefore disposal of untreated water into the water streams poses a substantial threat to the environment, such as deteriorating water quality, affecting aquatic life, and potentially posing harm to humans. Various techniques for the removal of dyes from water have been discussed in the literature, viz. membrane filtration [18], biological degradation [19], ion exchange [20], reverse osmosis [21], electrochemical oxidation [22], photocatalytic degradation [23], and adsorption [24]. Among these techniques, adsorption, using diverse adsorbents including low-cost biomass [10,18], hydrochars, and activated carbons fulfills the effective removal of dyes due to its ease of operation, lower selectivity towards the pollutants, and simplistic design [25–29].

The demand for efficient carbonaceous materials has boomed across the globe due to their multi-dimensional applications including energy storage, soil remediation, pharmaceutical delivery, and water treatment. Still, some drawbacks are related to the use of expensive and non-renewable precursors and high-energy processes in commercial production. These challenges underscore the need for the development of carbonaceous materials using energy-saving approaches and low-cost precursors, preferably renewable, such as biomass waste.

This work addresses the removal of dyes from wastewater by a diversity of adsorbents in its current state. The scalability of the adsorbent production method, for large-scale applications, is a limitation that has to be addressed further. Despite these challenges, the potential applications of the developed porous carbon materials in several water treatment scenarios, particularly in addressing dye contamination, are promising and warrant further investigation.

A promising source of waste biomass for porous carbon production and its utilization in dye removal is JFS. The Jamoya tree (Syzygium cumini), a member of the Myrtaceae

family, belongs to the Indian sub-continent; however, it is cultivated in the tropical and sub-tropical regions of the world [30]. Jamoya fruits are abundantly available in the Asian region, holding commercial value for culinary purposes [31]. Conversely, the fruit seeds lack utility or commercial value, serving as a source of solid biomass waste. To date, no study is available on the production of hydrothermally derived porous carbon from waste biomass (JFS). Being an inexpensive material, the use of Jamoya fruit seeds for their transformation into ACs contributes to waste management too. The utilization of HTC as an energy-efficient process contributes to energy conservation. In addition, the incorporation of Jamoya seeds in a circular economy framework will create environmental benefits through a reduction in waste and the promotion of sustainable practices [32]. Converting this underutilized biomass into value-added products has significant economic implications, further opening new prospects for renewable materials toward the broader goals of sustainability.

This study presents the production of hydrothermally derived JFS powder porous green carbon (JFS-PC) to remove CB from aqueous solutions, crucial to expand research in nutrition and the textile industry. An intensive characterization of the prepared materials was carried out to explore their textural and chemical properties. The role of functional groups, the substituents groups attached to the dyes, surface area, and surface charge of the adsorbent was highlighted in the adsorption. Kinetic models, isotherms, and thermodynamics parameters were performed and calculated to provide insights into the mechanism, sample nature, and features influencing the adsorption of the selected dyes.

2. Materials and Methods

2.1. Materials

In this study, Jamoya fruit seeds were collected locally. The seeds were washed several times to remove the adhered dust and impurities and dried in an oven at 60 °C for 24 h. The seeds were then ground and sieved to obtain a 10–30 mesh size and kept in a sealed plastic vial until its utilization. A Carmoisine B (CB) was purchased from Tokyo Chemical Industry (TCI), Tokyo, Japan. The NaOH and HCl used for the pH adjustments were supplied by Merck, Darmstadt, Germany. Double distilled water was used for the preparation of solutions throughout the work.

2.2. Preparation of Porous Green Activated Carbon

Jamoya fruit seeds (JFS) underwent hydrothermal carbonization, at a temperature of 230 °C, for 4 h in a PTFE lined hydrothermal reactor (Parr, Moline, Illinois, United States of America (USA)). The obtained JFS-based porous carbon, named JFS-HC, was stored in sealed plastic vials for future utilization. Porous green activated carbon was prepared by exposing 5 g of hydrothermally carbonized JFS (JFS-HC) to a heating rate of 5 °C min^{-1} until 850 °C in a tube furnace (Carbolite Gero, Hope Valley, United Kingdom) under CO_2 gas flow (400 mL min^{-1}) for 5 h [33]. The furnace was then cooled to room temperature under N_2 flow (100 mL min^{-1}), giving rise to a porous activated carbon (JFS-PC).

2.3. Proximate Analysis and pH at the Point of Zero Charge Determination

The proximate analysis of the biomass feedstock, derived hydrochar, and activated carbon provides significant information regarding the amount of volatile matter, ash, and moisture content. A high moisture content may reduce adsorption efficiency as it can block adsorption sites and may even interfere with the interactions between adsorbent and adsorbate. Volatile matter gives an indication of organic compounds decomposition. High ash indicates the presence of inorganic impurities which reduce adsorption efficiency. These analyses ensure the development of efficient porous carbon materials for specific ap-

plications. The volatile matter, ash, and moisture contents of JFS, JFS-HC, and JFS-PC were determined in accordance with the ASTM standard methods D3175-07 [34], E1755-01 [35], and D4442-07 [36], respectively. The pH_{pzc} of the samples was determined according to a method described by Carrott et al. [37].

2.4. Instrumental Methods

The ultimate analysis of the samples was performed primarily to confirm the carbonaceous nature of the precursor, ensuring the development of porous materials with high carbon content, which is generally beneficial for adsorption purposes. The analysis was performed using a CHNS analyzer (Vario Micro, Elementar, New York, NY, USA). Residual concentrations of CB in the solutions were determined using UV-Vis spectrophotometry (UV-1800, Shimadzu, Kyoto, Japan) at 518 and 521 nm, respectively. JFS, JFS-HC, and JFS-PC were evaluated by Fourier transform infrared spectroscopy (Spectrum Two, Perkin Elmer, Shelton, CT, USA) to evaluate the group functionality on their surface. Analyses were performed in the spectral region of 4000 to 400 cm^{-1}. N_2 adsorption–desorption measurements of the samples were taken using surface area analyzers at 77K (NOVA II and Autosorb iQ, Quantachrome, Boynton Beach, FL, USA). BET analysis was undertaken to determine the surface area, whereas the pore volume and average pore diameter of the samples were evaluated using the BJH method. X-ray diffraction (XRD) analysis was performed using a powder X-ray diffractometer (DMax-2200, Rigaku, Tokyo, Japan) equipped with copper radiation (Cu-Kα) working at 40 kV/40 mA. A 2θ range of 5–80°, with a scanning step of 0.02°, was selected for the analysis. Scanning electron microscopy (SEM) to evaluate the morphology of the samples was carried out using an EVO 18 Special Edition, Zeiss, Oberkochen, Germany microscope with an acceleration voltage ranging from 5 to 15 kV.

2.5. Batch Dyes Adsorption Experiments

Adsorption experiments in a one-component system were carried out as follows: 0.01 g adsorbent was added to 10 mL of dyes solution, with varying concentrations at the natural pH of the dye (5.3). The suspensions were left under agitation to equilibrium in a water bath shaker (JSGW, Ambala, India) with a temperature control feature at 25 °C. After reaching equilibrium, the mixture was separated using a Whatman filter paper, and the residual concentration of dyes that remained in the solution was evaluated using a UV-Vis spectrophotometer. UV-Vis spectrophotometry was used to measure dye concentration, with no sample interference since the solutions were synthetic and contained only CB dye. The instrument was regularly calibrated and blank (a blank was prepared with the adsorbent and distillated water) corrections along with replicate measurements minimized deviations. No significant absorbance variations were observed, ensuring the precision of dye concentration estimates. The equilibrium adsorption capacity (q_e) was calculated using the following formula:

$$q_e = \frac{C_i - C_e}{m} V \quad (1)$$

2.6. Statistical Analysis

The experimental data for the adsorption models and kinetics of the adsorption process were analyzed using Microsoft Excel to determine the correlation coefficients (R^2), which describe the goodness of fit. The experiments were performed in triplicate, and the R^2 values were used to assess the accuracy and reliability of the data.

3. Results and Discussion

3.1. Characterization of JFS, JFS-HC, and JFS-PC

The moisture, ash, and volatile matter contents, presented in Table 1, were found to be decreased upon hydrothermal carbonization and further activation process. The low moisture content could be ascribed to the carbonization of JFS at higher temperature while preparing the JFS-HC. The low volatile matter observed for the JFS-HC indicates the reduced particle density, which in turn is beneficial for applications in adsorption ultimate analysis (Table 1), showed a substantial increase in the carbon content of the JFS-PC, indicating that JFS can be utilized as an effective precursor for the production of porous carbons, mainly ACs. A comparison of ultimate analysis with other ACs available in the literature is provided in Table 1, which ensures the efficiency of developed porous carbon. The point of zero charge was determined in accordance with the method suggested by Carrott et al. [37] and was found to be 5.2, which reveals that the surface of JFS-PC is positively charged below pH 5.2, which will be beneficial for the interaction with contaminants anionic in nature, whereas it attracts cationic contaminants above pH 5.2. Therefore, it can be said that at pH < pHpzc, anionic pollutants are readily adsorbed by the developed ACs, whereas they favor the adsorption of cationic pollutants at pH > pHpzc.

Figure 1 depicts the FTIR spectra of JFS, JFS-HC, and JFS-PC. JFS showed a peak near 3400 cm^{-1}, ascribed to –OH stretching of hydroxyl groups. The band near 2900 cm^{-1} represents the C–H stretching vibration in the sample. The peak at 1587 cm^{-1} is attributed to the aromatic COOH and C–C groups in JFS. A peak at 1118 cm^{-1} refers to C–O–C stretching, confirming the presence of hemicellulose and cellulose in JFS [38]. A peak near 700 cm^{-1} represents the CH bending vibrations in JFS. JFS-HC showcases all the distinctive peaks of JFS with minor band shift and decrease in intensity; however, upon hydrothermal carbonization, few new peaks between 1600 and 1400 cm^{-1} emerged which may be attributed to the increase in the oxygenated functional groups during HTC. Interestingly, JFS-PC showed a smaller number of peaks which may be a consequence of the submission to a high temperature during activation. The peaks at 3450 and 2930 are assigned, respectively, to the OH and C–H stretching in the sample. The peaks at 1635 and 605 cm^{-1} are imputed to the aromatic COOH and C–H bending vibrations [39–41].

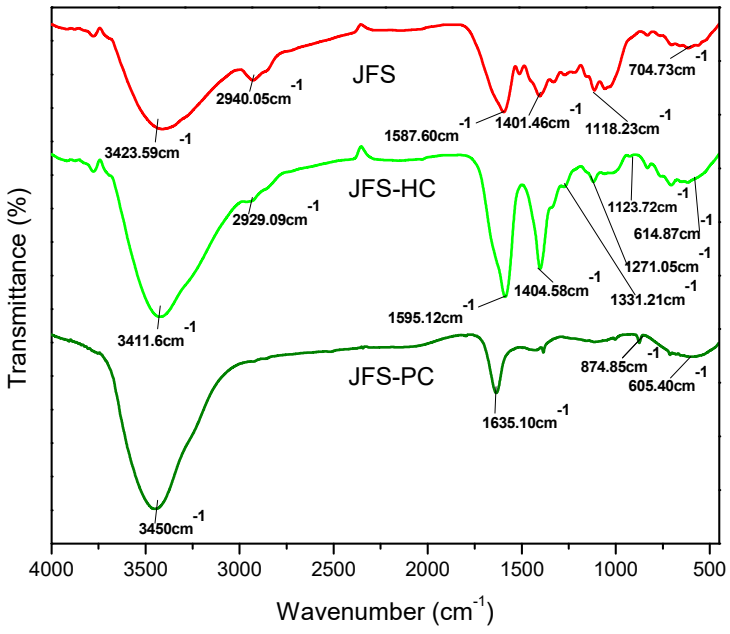

Figure 1. FTIR spectra of JFS, JFS–HC, and JFS–PC.

Figure 2 shows the XRD patterns of JFS-PC in comparison to JFS-HC and JFS samples. Two broad peaks at 2θ = 14° and 22.1°, attributed to (101) and (002) plane, were present in the case of JFS, which are the characteristic peaks of cellulose. A similar pattern was obtained with JFS-HC, indicating the retention of the original cellulosic structure of JFS despite undergoing HTC. In the case of JFS-PC, the characteristic peaks of cellulose become broader, indicating the formation of amorphous carbon material. Another strong peak seen at 2θ = 43° corresponds to (100) plane of graphite crystals, attributed to the interlayer condensation of graphite layers [42,43].

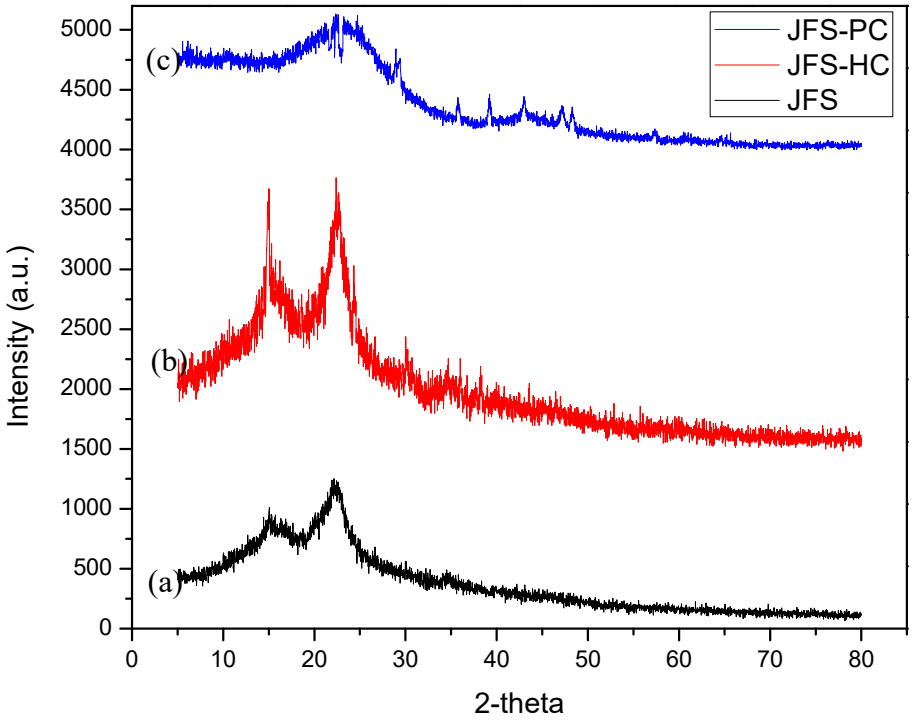

Figure 2. XRD patterns of (**a**) JFS, (**b**) JFS–HC, and (**c**) JFS–PC.

Figure 3 shows the SEM micrographs of JFS, JFS-HC, and JFS-PC, indicating that JFS has a smooth surface which converts to a rough surface with some pores and cracks upon HTC. Also, the formation of sphere-like structures was seen on the surface of JFS-HC (Figure 3b). The surface of the JFS-PC showed a porous surface with retention of the spherical structures (Figure 3c). The spherical structures indicate the hydrophobic nature of the prepared JFS-PC, which is beneficial for adsorption applications.

The N_2 adsorption–desorption isotherm shows a Type I curve with a short plateau ending at $p/p^\circ < 1$, and an upward deviation is observed in Figure 4, revealing wider micropores or mesopores contributing to the pore filling. The presence of a H4 hysteresis loop indicates that the capillary condensation is responsible for pore filling, and slit-shaped pores have been formed [44]. This is further confirmed by the textural properties (Table 2), which showed that the average pore diameter of JFS-PC is 3.97 nm, indicating the development of mesopores or wider micropores, facilitating the molecular diffusion of dye to the internal sites. Moreover, JFS-PC exhibited a high surface area (440.8 $m^2\ g^{-1}$) and pore volume (0.437 $cm^3\ g^{-1}$), both of which enhance the material's adsorptive performance. The adsorbent with a higher surface area can enhance the removal potential of JFS-PC owing to its ample active surface sites. In addition, the mesoporous structure of JFS-PC could give rise to the capability of adsorbing CB. The surface area of JFS and JFS-HC samples was also analyzed, and data presented in Table 2 reveals that both materials possess very low surface area when compared with JFS-PC, hence full isotherm was not given.

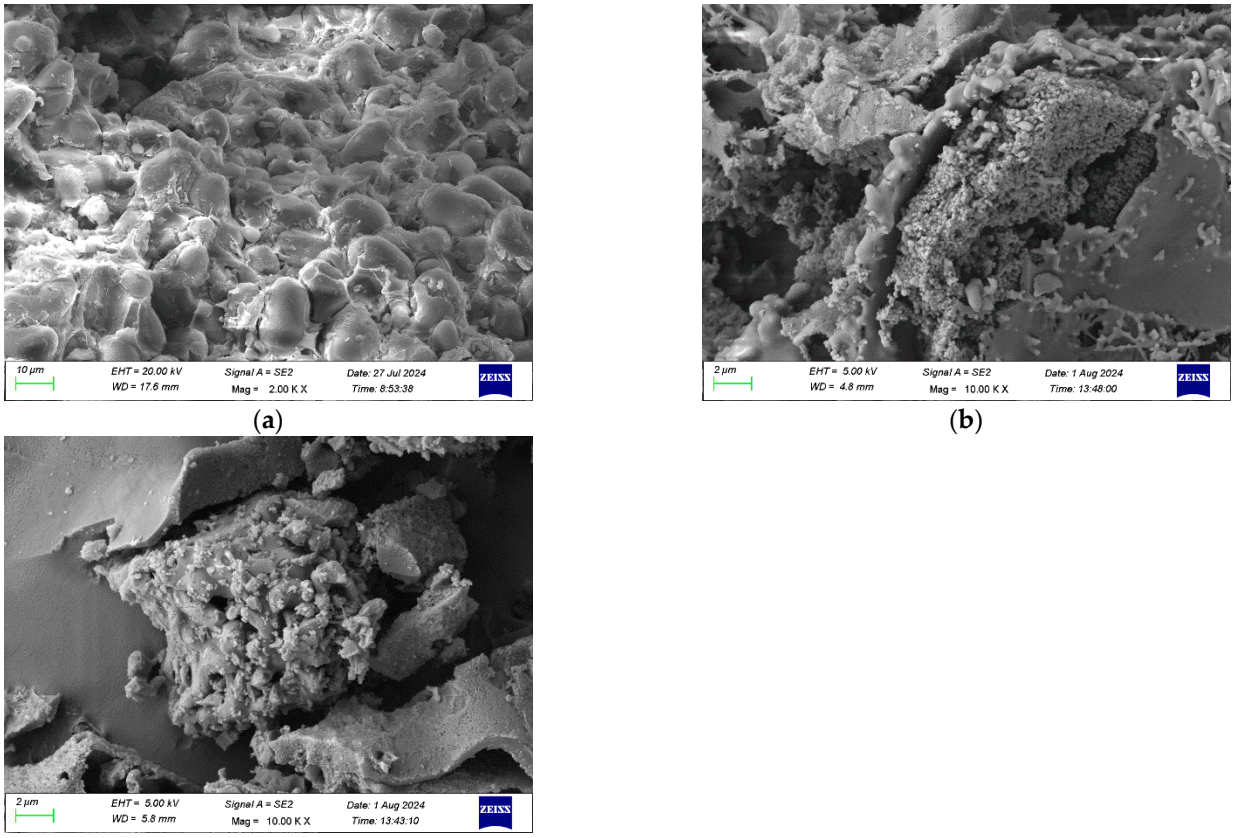

Figure 3. SEM micrographs of JFS (**a**), JFS-HC (**b**), and JFS-PC (**c**).

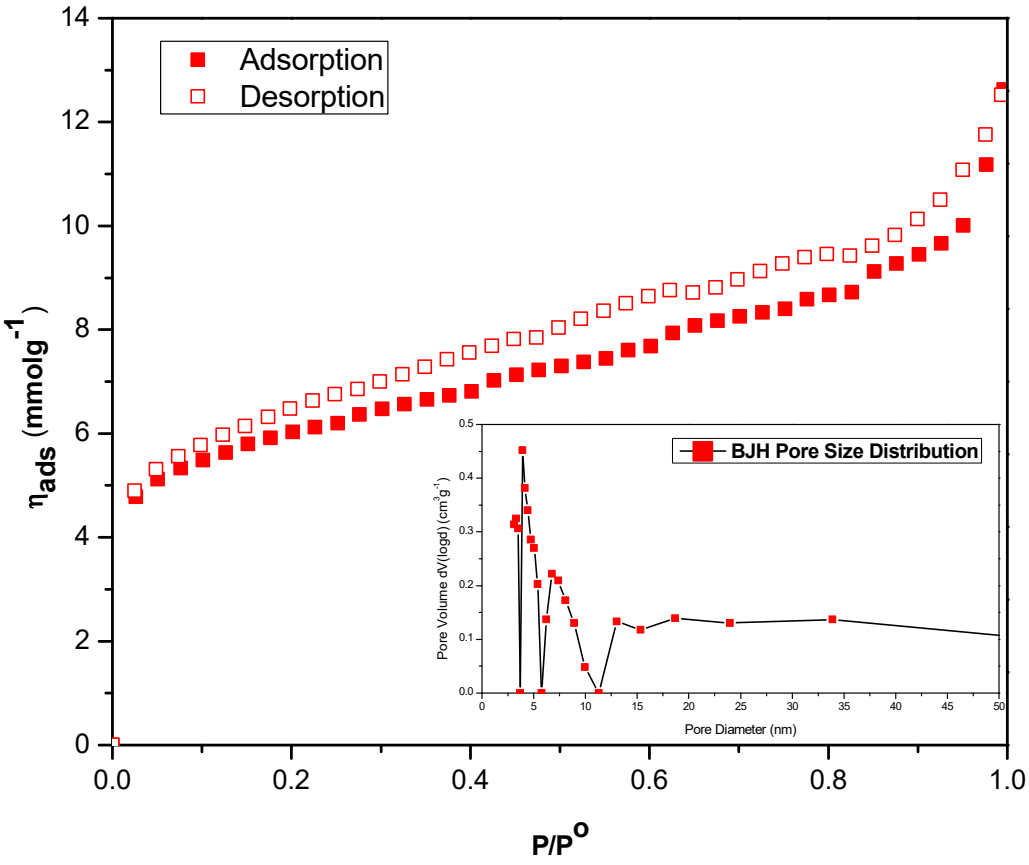

Figure 4. N_2 adsorption–desorption isotherms of JFS–PC.

3.2. Adsorption Studies

3.2.1. Effect of Contact Time, Initial Dye Concentration, and Solution pH

Figure 5 shows the adsorption equilibrium time profile for the removal of CB dye by JFS-PC at different initial dye concentrations (1×10^{-4} and 2×10^{-4} mol dm^{-3}). The equilibrium time, representing the time span necessary to attain equilibrium, was found to be 180 min. At this point, the dye desorption from JFS-PC reaches dynamic equilibrium with the adsorption process. Moreover, the obtained curves level off between 150 and 180 min, indicating monolayer adsorption. It is noteworthy that adsorption occurs rapidly initially and then slowly attains equilibrium. This may be attributed to the available vacant sites on JFS-PC initially which become saturated over time, resulting in increased time period [45]. Figure 5 also reveals that the adsorption of CB increases as its initial concentration increases. It may be attributed to the increase in collisions between dye and JFS-PC molecules at higher concentrations. Moreover, an increase in the driving force of concentration gradient reduced the mass transfer resistance of CB between the liquid and the JFS-PC adsorbent [46].

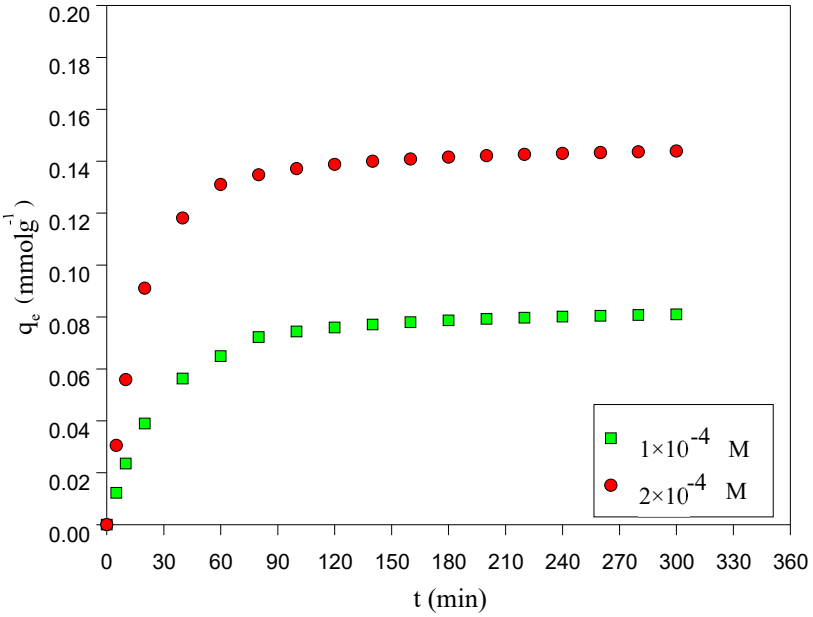

Figure 5. Influence of contact time and initial concentration on the removal of CB by JFS−PC at 25 °C.

Solution pH directly affects the adsorption of dyes and therefore it is crucial to investigate its impact on the process. Figure 6 displays the experimental results concerning the effect of the pH of the solution on the adsorption of CB by JFS-PC. It was seen that the extent of removal of the dye was highly influenced, with varying pH due to its effect on the binding sites of the adsorbent and the ionization of CB molecules. The adsorption capacity of JFS-PC decreases with an increase in pH from 2 to 12; however, a minor difference in the adsorption capacity was observed between pH 2 and 5. Since JFS-PC exhibits enhanced adsorption of CB under pH levels between 2 and 5, the natural pH (5.3) of the dye solution was selected as optimum pH for the experimental investigations. In the acidic pH range, the surface of the JFS-PC is positively charged (pHpzc—5.5), thereby attracting the negatively charged molecules of CB. The higher adsorption of the dye is also supported by the increased protonation. This promotes the dye's affinity for active sites and accelerates the diffusion process. Meanwhile, in an alkaline pH range, protonation is reduced, and the hydroxyl ion concentration dominates in the solution. The OH^- ions compete with the dye molecules for the adsorption sites, thereby retarding and reducing the adsorption of CB.

The surface of the JFS-PC is also negatively charged in the alkaline pH range, resulting in reduced adsorption owing to the repulsion of the dye molecules.

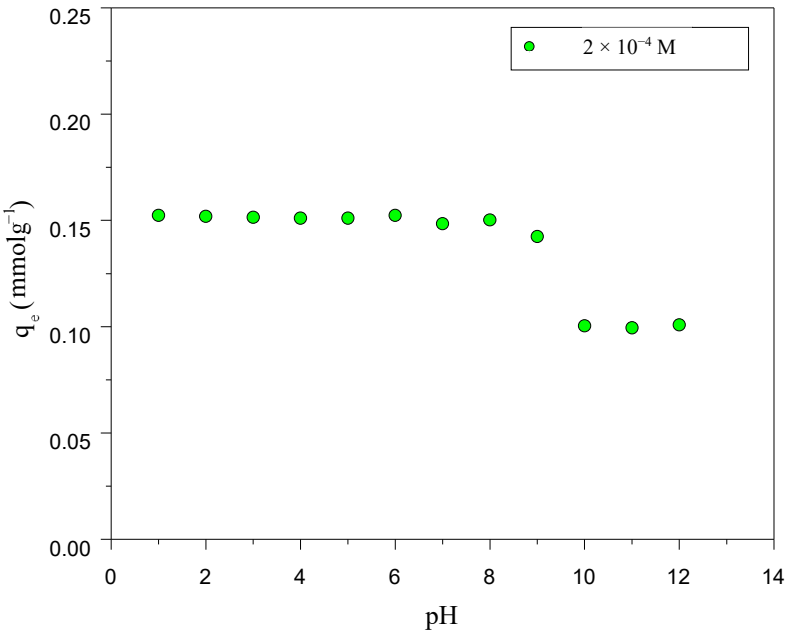

Figure 6. Influence of pH on the removal of CB by JFS−PC at 25 °C (Carmoisine B initial concentration: 2×10^{-4} mol dm^{-3}).

3.2.2. Adsorption Isotherms and Thermodynamics Studies

The relationship between the equilibrium concentration of CB and the equilibrium adsorption capacity of JFS-PC at different temperatures (25, 35, and 45 °C) was investigated, and the experimental data were fitted and analyzed using the Langmuir, Freundlich, Temkin, and Dubinin–Radushkevich (D-R) models. The associated equations and the corresponding parameters for the above models are given in Table 3. As depicted in Figure 7 and Table 4, the adsorption capacity significantly increased and then gradually reached equilibrium with an increasing concentration of CB at 25, 35, and 45 °C. Figure 7 shows that CB adsorption increased with increasing temperature. As shown in Figure 8a–d and Table 4, the Langmuir adsorption capacity closely related to the experimental values obtained at 25, 35, and 45 °C (0.310, 0.324, and 0.334 mmol g^{-1}, respectively), and the co-relation coefficient (R^2 = 0.993 to 0.998) for the Langmuir model was higher than that of all the other applied models. This indicates that the JFS-PC surface has uniform adsorption energy for the modeled dye. The adjustment made with the DR equation was the one that gave a lower correlation coefficient. Consequently, the dye adsorption process can be best described through a monolayer adsorption mechanism. A comparison of the adsorption capacity and best-fitting isotherm model of JFS-PC with other activated carbons, available in the literature, is provided in Table 5.

Figure 9 presents the Gibb's free energy (ΔG°), entropy (ΔS°), and enthalpy (ΔH°) values obtained through the calculation of the Van't Hoff equation (Table 3), and the obtained parameters are given in Table 6. The positive ΔH° value and negative ΔG° value suggest that the adsorption of CB by JFS-PC is an endothermic and spontaneous process [47]. Meanwhile, the gradual increase in values of free energy with increasing temperature indicates that high temperatures favor the adsorption of CB by JFS-PC [48]. The positive ΔS° value indicates an increase in the degree of disorder at the solid–liquid interface during the adsorption process.

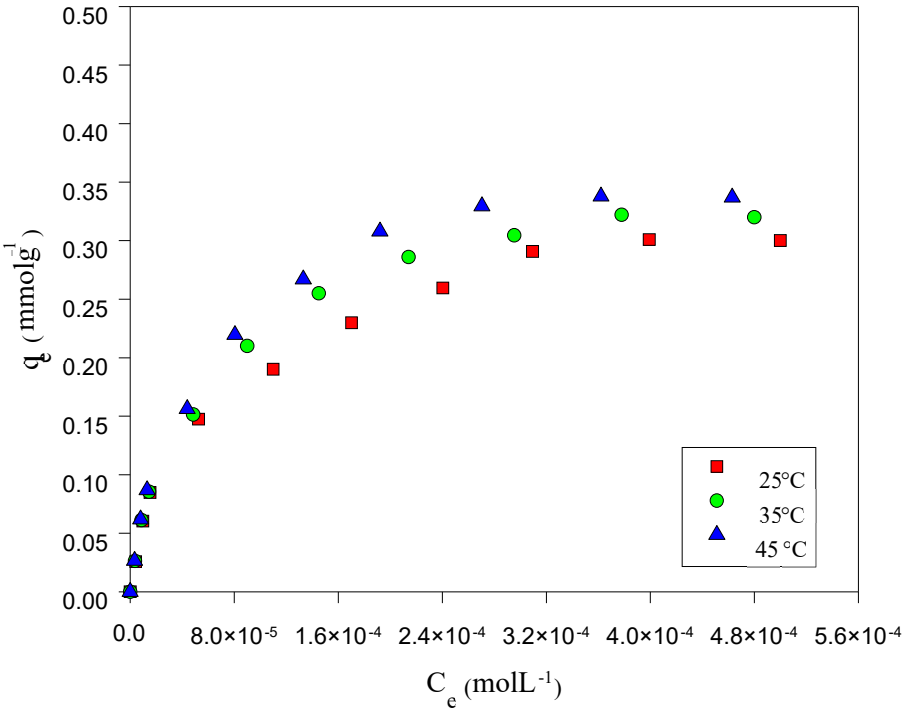

Figure 7. Experimental adsorption isotherm for the removal of CB by JFS−PC at different temperatures.

(**a**)

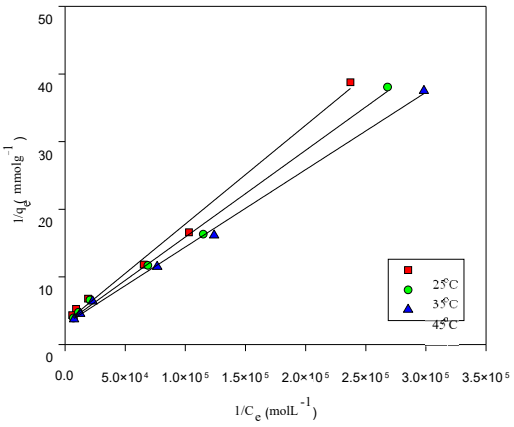

(**b**)

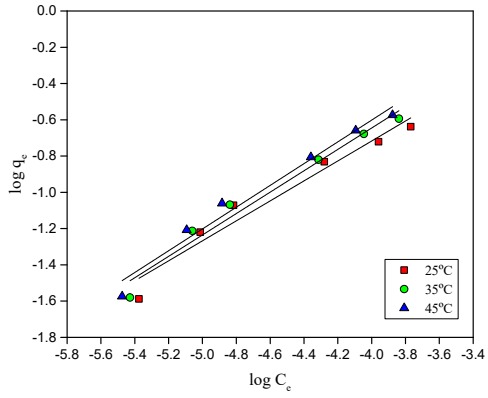

(**c**)

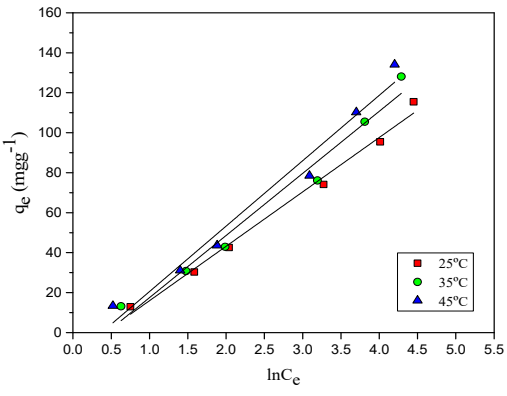

(**d**)

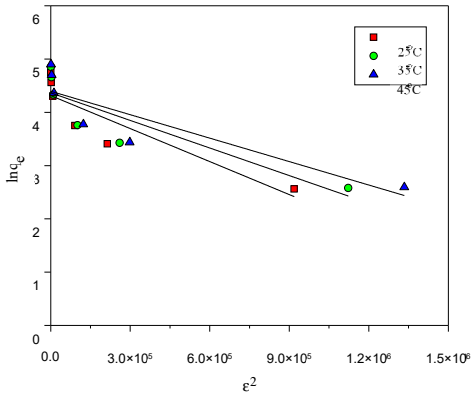

Figure 8. (**a**) Langmuir isotherm, (**b**) Freundlich isotherm, (**c**) Temkin isotherm, and (**d**) D-R isotherm for the removal of CB by JFS-PC at different temperatures.

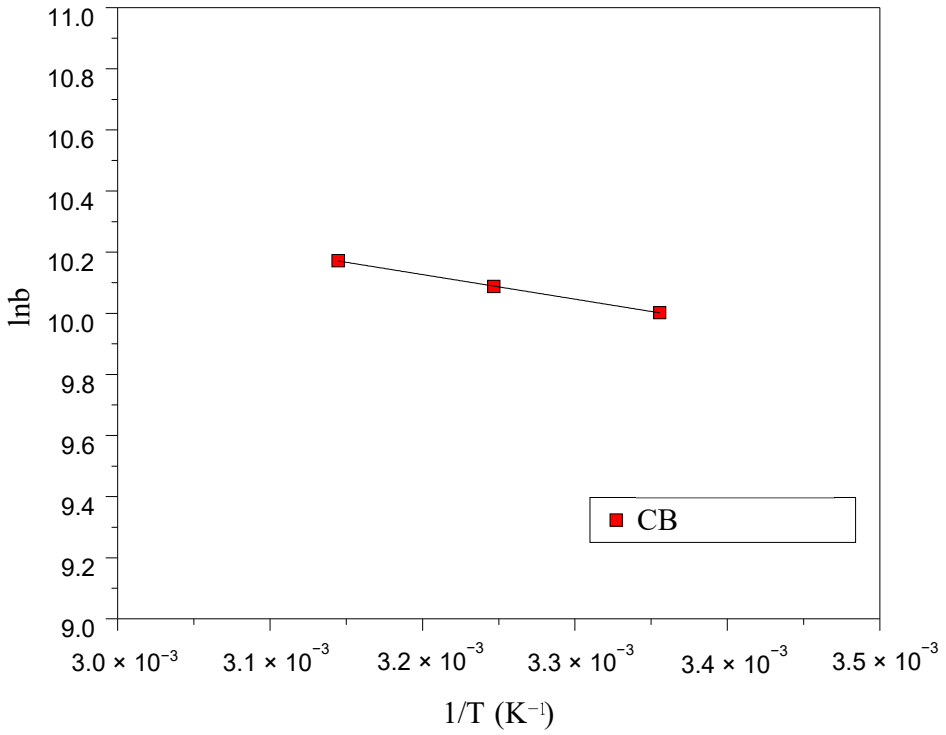

Figure 9. Van't Hoff plot for the removal of CB by JFS-PC.

3.2.3. Mechanism

The surface of JFS-PC exhibits ample adsorption sites which facilitate the binding of CB. Point of zero charge (pHpzc) investigations of JFS-PC revealed that the JFS-PC's surface exhibits a positive charge when subjected to acidic pH conditions. Consequently, this surface with positive charge has the ability to form electrostatic interactions with CB dye molecules [49], facilitating the binding to JFS-PC. The molecules of CB dye have a negatively charged structure due to the presence of sulphonate and hydroxyl groups in its structure which also enhances the extent of binding through electrostatic attraction of CB with the adsorbent below pH 5.2. The surface of JFS-PC has different functional groups, including carboxylic and –OH, which can serve as active sites for binding with $SO_3^-Na^+$ and N^+ of the CB dye [50]. This binding is supported via different mechanisms viz. electrostatic interactions and H-bonding. In addition, the contaminants having a benzene ring generally have strong affinity to adsorb onto the surface of carbon rich materials owing to the interactions between C=C of JFS-PC and the benzene ring of the CB via π- π interactions [51].

The porous character of JFS-PC is crucial for the adsorption of the dyes from water. The high surface area (440.8 m^2g^{-1}) of JFS-PC and high porosity (0.437 cm^3g^{-1}) allows the molecules of CB to adsorb on the JFS-PC surface. Therefore, the aforementioned mechanisms may be attributed to the higher adsorption of CB onto the JFS-PC surface. A pictorial representation for the possible mechanisms, responsible for the adsorption of CB onto JFS-PC, is shown in Figure 10.

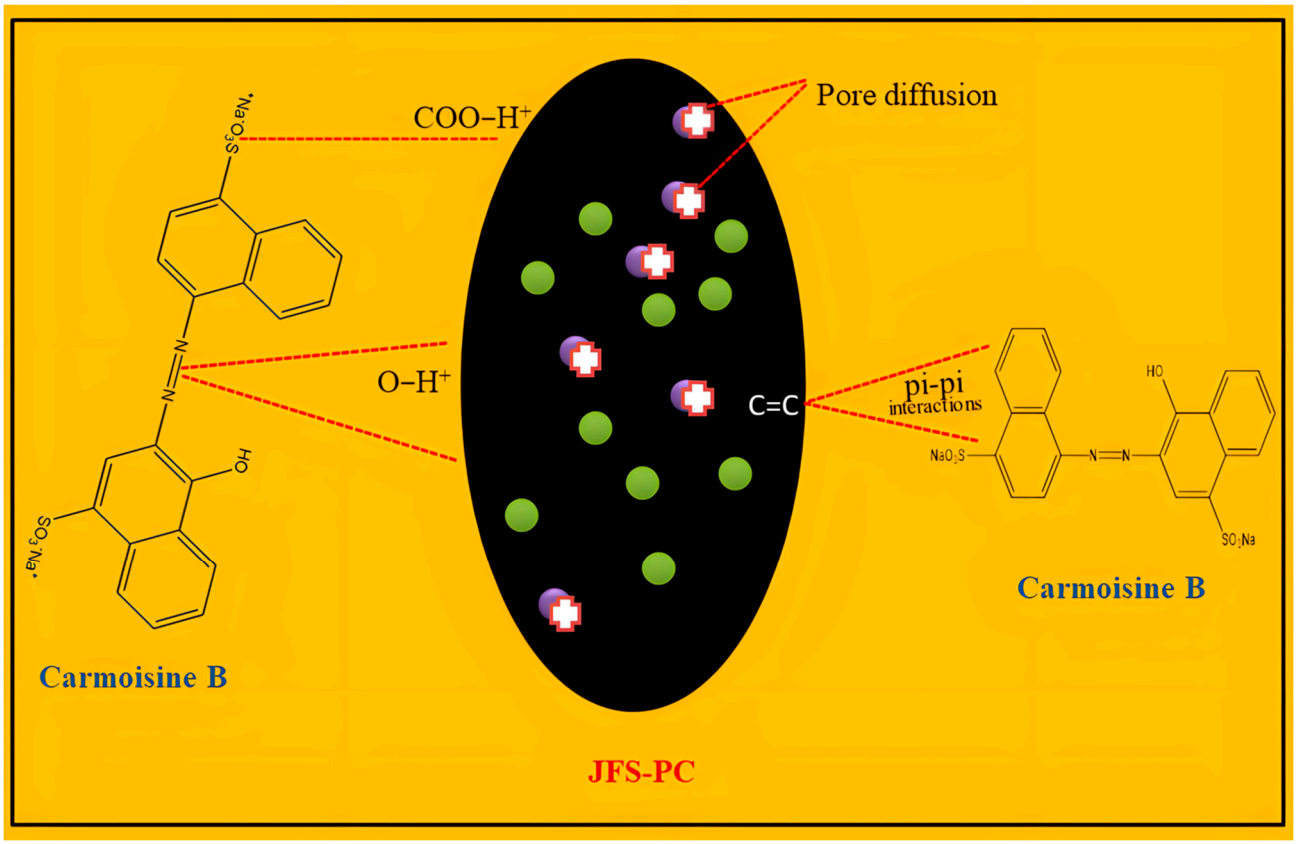

Figure 10. Possible mechanism route for the adsorption of CB onto JFS-PC surface.

3.2.4. Kinetic Investigations

To understand the adsorption mechanism of JFS-PC for CB, an in-depth analysis of adsorption kinetics was carried out and the details with corresponding parameters for the applied models (pseudo-first-order (PFO), pseudo-second-order (PSO), and Elovich models) are given in Table 3. As depicted in Figure 11a–c, and Table 7, the experimental data were fitted using PFO, PSO, and Elovich models. The fitting correlation coefficient ($R^2 \geq 0.9861$) of the PSO model was higher than those obtained with the PFO and Elovich models ($R^2 \geq 0.7229$), and the experimental adsorption values were similar to the calculated values. This reveals that the adsorption kinetics of CB on JFS-PC is in close agreement with the PSO model.

The involved mechanism and the rate governing step were further elucidated by applying the intraparticle diffusion model (IPD) to the experimental data. The intraparticle diffusion model in Figure 11d and Table 7 shows the multi-stage sorption of CB onto developed JFS-PC. The first stage describes the transfer of CB from the bulk of the solution to the JFS-PC's surface, whereas the second stage denotes the penetration of CB molecules into the JFS-PC's pores. In addition, the line in Figure 11d does not pass by the origin, affirming that some other mechanism along with IPD is involved in the CB adsorption by JFS-PC [52]. A comparison of kinetic studies of the current work with the results obtained on the use of other activated carbons for the removal of dyes is provided in Table 5. Maximum research works indicate that the pseudo-second-order model is the best fit to describe the kinetics, which is in line with the findings of our study.

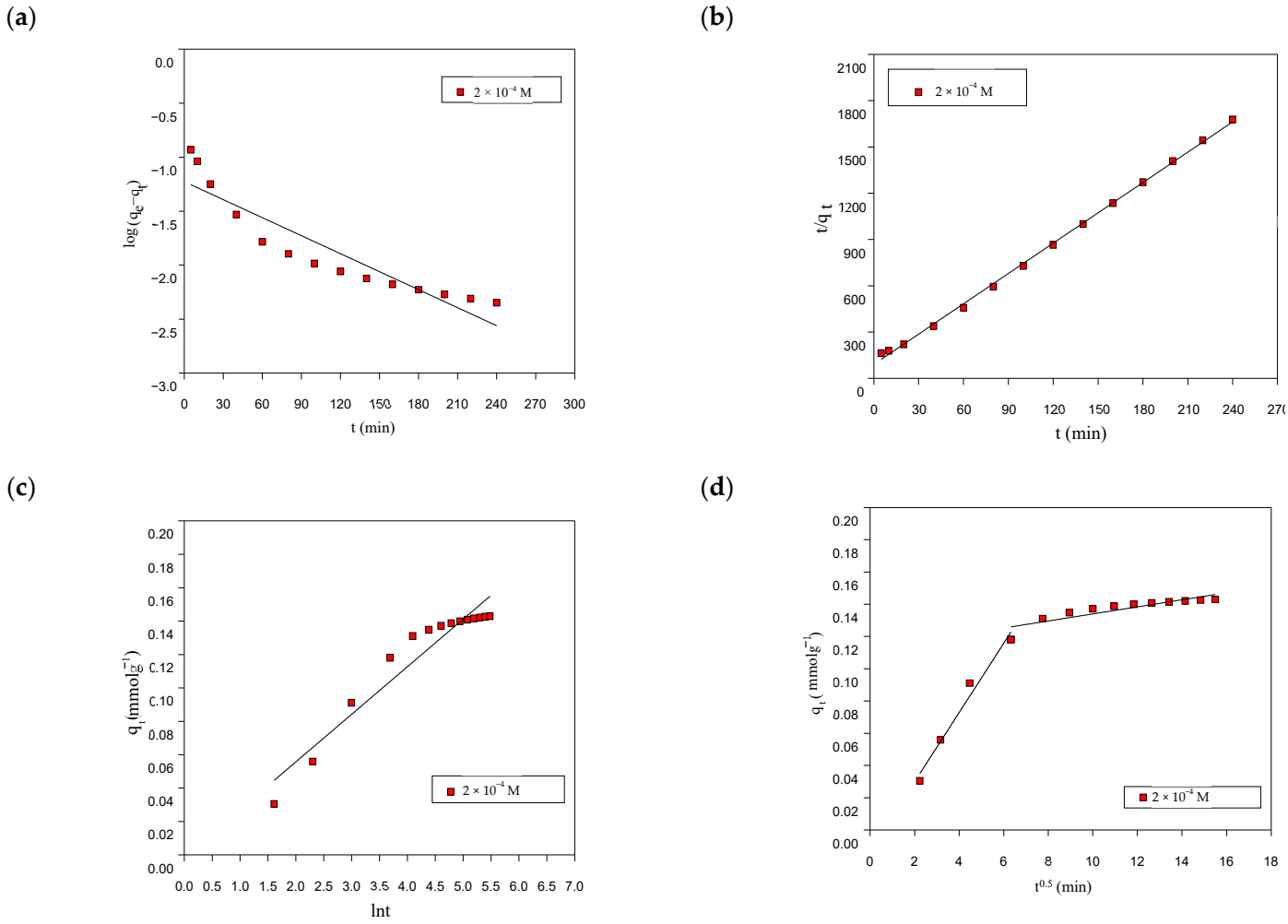

Figure 11. (**a**) PFO, (**b**) PSO, (**c**) Elovich, and (**d**) IPD kinetic models for the removal of CB by JFS-PC at 25 °C.

Table 1. Proximate and ultimate analysis of JFS, JFS-HC, and JFS-PC and comparison with the other activated carbon available in the literature.

Proximate Analysis (%)	**Moisture Content**	**Ash Content**	**Volatile Matter**		**Reference**
JFS	68.32	6.56	2.89		This study
JFS-HC	58.11	6.23	2.43		This study
JFS-PC	-	0.51	—		This study
Activated carbon from apricot stones	-	2.10	-		[6]
Activated carbon from almond shell	-	0.5	-		[8]
Activated carbon from sugarcane baggase	-	1.65	-		[53]
Activated carbon from thin walnut shell	-	5.01	-		[54]
Ultimate Analysis (%)	**C**	**H**	**N**	**S**	**Reference**
JFS	44.12	7.12	0.92	0.87	This study
JFS-HC	62.34	4.32	0.04	0.02	This study
JFS-PC	84.21	1.20	0.02	0.03	This study
Activated carbon from almond shell	58.78	3.26	1.25	0.07	[8]
Activated carbon from apricot stones	82.76	-	-	-	[6]
Activated carbon from Phyllanthus emblica	70.23	2.98	0.64	0.41	[12]
Activated carbon from orange peel	83.9	1.9	0.4	-	[33]
Activated carbon from cupuassu	74.16	2.32	0.66	-	[50]
Activated carbon from Brazilian nut shell	71.30	2.65	1.03	-	[50]

Table 2. Textural properties of JFS, JFS-HC, JFS-PC.

Materials	Surface Area (m^2 g^{-1})	Average Pore Size (nm)	Total Pore Volume (cm^3 g^{-1})
JFS	2.40	6.05	0.004
JFS-HC	10	3.40	0.027
JFS-PC	440.8	3.97	0.437

Table 3. Isotherm models, kinetics, and thermodynamics equations.

Models	Mathematical Expression	Plot Axis	Evaluated Parameters	Description	Reference
Isotherm Models					
Langmuir	$1/q_e = 1/q_{max} + 1/q_{max}bC_e$ $R_L = 1/1+bC_o$	$1/q_e$ vs.$1/C_e$	q_{max} and b	C_e; adsorbate concentration at equilibrium q_e (mmol g^{-1}); amount of pollutant adsorbed at C_e q_{max} (mmol g^{-1}); Monolayer adsorption capacity of JFS-PC. b (L mol^{-1}); Langmuir adsorption coefficient	[55]
Freundlich	$\log q_e = \log K_f + (1/n) \log C_e$	$\log q_e$ vs.$\log C_e$	K_f and n	C_e; adsorbate concentration at equilibrium q_e(mmol g^{-1}); amount adsorbed at C_e K_F (mmol g^{-1}) and n; Freundlich constant affiliated to the adsorption capacity and heterogeneity, respectively.	[56]
Temkin	$q_e = B_T \ln K_T + B_T \ln C_e$ $B_T = RT/b_T$	q_e vs. $\ln C_e$	K_T and B_T	B_T; heat of adsorption b_T (J mol^{-1}); constant related to the heat of adsorption K_T (L mg^{-1}); Temkin constant	[57]
D-R	$\ln q_e = \ln q_m - \beta_{DR} \varepsilon^2$ $\varepsilon = RT \ln(1+1/C_e)$	$\ln q_e$ vs. ε^2	Q_m and β_{DR}	q_m (mg g^{-1}); D-R monolayer capacity β_{DR} (mol^2 kJ^{-2}); constant related to the adsorption energy ε; Polanyi potential	[58]
Kinetic Models					
PFO	$\log(q_e - q_t) = \log q_e - \frac{K1}{2.303} t$	$\log(q_e - q_t)$ vs. t	Q_e and k_1	q_e and q_t (mmol g^{-1}); adsorbed amount of CB at equilibrium and at time t, respectively. k_1; PFO rate constant of adsorption	[59]
PSO	$\frac{t}{q_t} = \frac{1}{k_2 q_e^2} + \frac{1}{q_e} t$	$\frac{t}{q_t}$ vs. t	Q_e and k_2	q_e and q_t (mmol g^{-1}); adsorbed amount of CB at equilibrium and at time t, respectively. k_2; PSO rate constant of adsorption	[60]
Elovich	$qt = 1/\beta \ln(\alpha\beta) + 1/\beta \ln(t)$	q_t vs. ln(t)	α and β	β (g $mmol^{-1}$); desorption rate constant α (mmol g^{-1} min^{-1}); initial adsorption rate constant q_t (mmol g^{-1}); adsorption capacity at time t	[61]
Intraparticle Diffusion Model	$q_t = K_{id} \cdot \sqrt{t} + C$	q_t vs. $\sqrt{t}$	K_{id} and C	q_t (mmol g^{-1}); adsorption capacity at time t K_{id}; rate constant of intraparticle diffusion C; intercept of intra particle diffusion	[62]
Thermodynamics Equations					
Gibb's Free Energy	$\Delta G^\circ = -R T \ln(b)$		ΔG°	T; temperature, b (L mol^{-1}) and R are the Langmuir adsorption and universal gas constants, respectively, ΔG°; change in free energy of the adsorption system	
Van't Hoff	$\ln b = -\Delta H^\circ/RT + \Delta S^\circ/R$	lnb vs.1/T	ΔH° and ΔS°	T; temperature, b (L mol^{-1}), and R are the Langmuir adsorption and universal gas constants, respectively, ΔH°; change in enthalpy, ΔS°; change in entropy	[63]

Table 4. Parameters of Langmuir, Freundlich, D-R, and Temkin isotherm models at different temperatures for CB dye adsorption onto JFS-PC surface.

Adsorbate/ Temperature	Experimental		Langmuir			Freundlich			D-R			Temkin		
	q_{exp} (mg g^{-1})	q_{exp} (mmol g^{-1})	q_{max} (mmol g^{-1})	q_{max} (mg g^{-1})	b (L mol^{-1})	R^2	K_f (mmol g^{-1})	n	R^2	q_m (mg g^{-1})	E (kJ mol^{-1})	R^2	A_t (L mg^{-1})	b (kJ mol^{-1})	R^2
CB/25 °C	153	0.291	0.310	156	2.21×10^{-4}	0.993	30.7	1.82	0.953	74.8	0.492	0.814	0.662	0.091	0.990
CB/35 °C	162	0.305	0.324	163	2.40×10^{-4}	0.995	51.9	1.69	0.972	78.7	0.538	0.787	0.646	0.079	0.975
CB/45 °C	169	0.329	0.334	168	2.62×10^{-4}	0.998	63.1	1.66	0.975	81.1	0.584	0.777	0.689	0.076	0.973

Table 5. Comparison of JFS-PC with other ACs available in the literature for the removal of dyes.

Precursor	Activation Temperature (°C)	Surface Area (m^2 g^{-1})	Target Adsorbate	Adsorption Capacity (mg g^{-1})	Isotherm Model Applied	Kinetic Model Applied with Rate Constant and Mechanism	Reference
Factory-rejected tea waste	800	368.92	Methylene Blue	487.4	Langmuir	Pseudo-second-order K_2—0.214 g. $mg^{-1}min^{-1}$ Contact time—0.5–25 h Mechanism–film and intraparticle diffusion	[64]
Pine needle	-	-	Malachite Green	97.08	Langmuir	Pseudo-second-order K_2—2.21×10^{-3} g. $mg^{-1}min^{-1}$ Contact time—180 min Mechanism–intraparticle Diffusion, film diffusion, and boundary layer control	[65]
Chickpea stem	600	455	Methylene Blue	887	Langmuir	-	[66]
Carnauba leaves	500	402.43	Rhodamine B	35.06	Freundlich	Pseudo-second-order K_2—0.236 g. $mg^{-1}min^{-1}$ Contact time—120 min	[67]
Pine nut shells	500	296.01	Rhodamine B	29.62	Freundlich	Pseudo-second-order K_2—0.299 g. $mg^{-1}min^{-1}$ Contact time—120 min	[67]
Apricot stone	700	359.40	Methylene Blue	36.68	Langmuir	Pseudo-second-order K_2—0.721 g. $mg^{-1}min^{-1}$ Contact time—130 min Mechanism–chemisorption and intraparticle diffusion	[6]
Almond shell	450	733	2,4,6-trinitrophenol	74.03	Sips	Pseudo-second-order K_2—0.016 g. $mg^{-1}h^{-1}$ Mechanism–chemical sorption	[8]
Jamoya fruit seeds	850	440.8	Carmoisine B	153	Langmuir	Pseudo-second-order	This study

Table 6. Thermodynamic parameters for CB dye adsorption onto JFS-PC surface.

Dye	Temperature (°C)	ΔG° (kJ mol^{-1})	ΔS° (J mol^{-1} K^{-1})	ΔH° (kJ mol^{-1})
CB	25	−24.8	105.6	6.69
	35	−25.8		
	45	−26.9		

Table 7. Parameters of PFO, PSO, Elovich, and Intraparticle diffusion model for CB dye adsorption onto JFS-PC surface.

Kinetic Model	Parameters	Conc. (2×10^{-4})
Experimental	q_e (mmol g^{-1})	0.147
PFO	q_e (cal) (mmol g^{-1})	0.0592
	K_1 (min^{-1})	0.0128
	R^2	0.855
PSO	q_e (cal) (mmol g^{-1})	0.1526
	K_2 (g $mmol^{-1}$ min^{-1})	0.477
	R^2	0.998
Elovich	α (mmol $g^{-1}min^{-1}$)	0.0273
	β (g $mmol^{-1}$)	35.09
	R^2	0.923
IPD	K_{p1}	0.022
	C_1	0.013
	R^2	0.975
	K_{p2}	0.0022
	C_2	0.112
	R^2	0.794

4. Conclusions

In summary, an effective adsorbent from an inexpensive and sustainable precursor, Jamoya fruit seeds, using hydrothermal carbonization and physical activation has been successfully developed for efficiency and tested for the removal of CB dye from the aqueous phase. Characterization of the prepared adsorbent along with the precursor and hydrochar was performed. Elemental composition showed that the prepared adsorbent was rich in carbon. The textural and chemical characteristics determined by means of FTIR, XRD, SEM, and BET analysis indicate that JFS-PC can be efficiently used for adsorption applications. pH analysis showed that the adsorption was enhanced in an acidic pH range as the

surface of the adsorbent holds positive charge below pH 5.2 (pHpzc—5.2). It achieves a maximum Langmuir adsorption capacity of 168 mg g^{-1} for CB at 45 °C. Mechanism analysis revealed that pore diffusion, electrostatic interactions, H-bonding, and π- π interactions governed the adsorption process. Thermodynamics findings revealed the endothermic and physisorption nature of the process. Kinetic adsorption of Carmoisine B followed a pseudo-second-order model. A hydrothermal route for the development of porous carbons was found to be energy efficient as mild temperature was used during the process. The fact that no hazardous gases are emitted during HTC makes it environmentally friendly compared to the conventional methods. This work not only provides an alternative for environmental remediation, through the treatment of dye-contaminated water, but it paves the way for the management of organic solid waste too. The potential of the developed material for the removal of different pollutants, such as emerging contaminants, pharmaceutical contaminants, and fertilizers, can be explored in future works.

Author Contributions: Conceptualization, S. and S.C. (Shubham Chaudhary); methodology, S.C. (Shubham Chaudhary) and S.; software, S. and, S.C. (Shubham Chaudhary); validation, S.C. (Shubham Chaudhary), M.C., and S.; formal analysis, M.C., S.C. (Shubham Chaudhary), and S.; investigation, S.C. (Shubham Chaudhary) and S.; resources, I.P.d.P.C. and S.; data curation, S. and S.C. (Shubham Chaudhary); writing—original draft, S.C. (Shubham Chaudhary). and S.; writing—review and editing, V.T., S.C. (Shivangi Chaubey), I.P.d.P.C., S.C. (Shubham Chaudhary), M.C., and S.; visualization, S.C. (Shivangi Chaubey), M.C., V.G., J.A., and S.; supervision, S. All authors have read and agreed to the published version of the manuscript.

Funding: This research received no external funding.

Data Availability Statement: The data of this study is available upon reasonable request to the corresponding authors.

Acknowledgments: The authors are thankful to DST, New Delhi, India, for the financial support. One of the authors (Jahangeer Ahmed) would like to extend his sincere appreciation to the Researchers Supporting Project number (RSP2025R391), King Saud University, Riyadh, Saudi Arabia.

Conflicts of Interest: The authors declare no conflicts of interest.

References

1. Eslamipoor, R. A fuzzy multi-objective model for supplier selection to mitigate the impact of vehicle transportation gases and delivery time. *J. Data Inf. Manag.* **2022**, *4*, 231–241. [CrossRef]
2. de Andrade, R.C.; Menezes, R.S.G.; Fiuza, R.A., Jr.; Andrade, H.M.C. Activated carbon microspheres derived from hydrothermally treated mango seed shells for acetone vapor removal. *Carbon Lett.* **2021**, *31*, 779–793. [CrossRef]
3. Mbarki, F.; Selmi, T.; Kesraoui, A.; Seffen, M. Low-cost activated carbon preparation from Corn stigmata fibers chemically activated using H_3PO_4, $ZnCl_2$ and KOH: Study of methylene blue adsorption, stochastic isotherm and fractal kinetic. *Ind. Crops Prod.* **2022**, *178*, 114546. [CrossRef]
4. Gupta, V.K.; Carrott, P.J.M.; Ribeiro Carrott, M.M.L.; Suhas. Low-Cost adsorbents: Growing approach to wastewater treatment—A Review. *Crit. Rev. Environ. Sci. Technol.* **2009**, *39*, 783–842. [CrossRef]
5. Zhang, J.; Duan, C.; Huang, X.; Meng, M.; Li, Y.; Huang, H.; Wang, H.; Yan, M.; Tang, X. A review on research progress and prospects of agricultural waste-based activated carbon: Preparation, application, and source of raw materials. *J. Mater. Sci.* **2024**, *59*, 5271–5292. [CrossRef]
6. Djilani, C.; Zaghdoudi, R.; Djazi, F.; Bouchekima, B.; Lallam, A.; Modarressi, A.; Rogalski, M. Adsorption of dyes on activated carbon prepared from apricot stones and commercial activated carbon. *J. Taiwan Inst. Chem. Eng.* **2015**, *53*, 112–121. [CrossRef]
7. Yadav, S.K.; Dhakate, S.R.; Pratap Singh, B. Carbon nanotube incorporated eucalyptus derived activated carbon-based novel adsorbent for efficient removal of methylene blue and eosin yellow dyes. *Bioresour. Technol.* **2022**, *344*, 126231. [CrossRef]
8. Mohan, D.; Sarswat, A.; Singh, V.K.; Alexandre-Franco, M.; Pittman, C.U. Development of magnetic activated carbon from almond shells for trinitrophenol removal from water. *Chem. Eng. J.* **2011**, *172*, 1111–1125. [CrossRef]
9. Cheng, J.; Bi, C.; Zhou, X.; Wu, D.; Wang, D.; Liu, C.; Cao, Z. Preparation of bamboo-based activated carbon via steam activation for efficient methylene blue dye adsorption: Modeling and mechanism studies. *Langmuir* **2023**, *39*, 14119–14129. [CrossRef]

10. Cansado, I.P.P.; Geraldo, P.F.; Mourão, P.A.M.; Castanheiro, J.E.; Carreiro, E.P.; Suhas. Utilization of biomass waste at water treatment. *Resources* **2024**, *13*, 37. [CrossRef]
11. Jain, A.; Balasubramanian, R.; Srinivasan, M.P. Hydrothermal conversion of biomass waste to activated carbon with high porosity: A review. *Chem. Eng. J.* **2016**, *283*, 789–805. [CrossRef]
12. Sevilla, M.; Maciá-Agulló, J.A.; Fuertes, A.B. Hydrothermal carbonization of biomass as a route for the sequestration of CO_2: Chemical and structural properties of the carbonized products. *Biomass Bioenergy* **2011**, *35*, 3152–3159. [CrossRef]
13. Suhas; Gupta, V.K.; Singh, L.P.; Chaudhary, M.; Kushwaha, S. A novel approach to develop activated carbon by an ingenious hydrothermal treatment methodology using Phyllanthus emblica fruit stone. *J. Clean. Prod.* **2021**, *288*, 125643. [CrossRef]
14. Chung, K.-T. Azo dyes and human health: A review. *J. Environ. Sci. Health Part C* **2016**, *34*, 233–261. [CrossRef]
15. Gupta, V.K.; Suhas. Application of low-cost adsorbents for dye removal—A review. *J. Environ. Manag.* **2009**, *90*, 2313–2342. [CrossRef] [PubMed]
16. India Azo Dyes Market Competition Forecast & Opportunities. 2023. Available online: https://www.researchandmarkets.com/report/india-azo-dye-Market#:~:text=The%20India20Azo%20Dyes%20Market%20achieved%20a%20volume,at%20volume%20of%2011.07%20thousand%20tonnes%20by%202029 (accessed on 15 September 2024).
17. Nazar, M.F.; Murtaza, S.; Ijaz, B.; Asfaq, M.; Mohsin, M.A. Photophysical investigations of carmoisine interacting with conventional cationic surfactants under different pH conditions. *J. Dispers. Sci. Technol.* **2015**, *36*, 18–27. [CrossRef]
18. Wan, H.; Zhu, X.; Wang, J.; Cao, F.; Zhang, Y.; Yao, Z.; Wang, S.; Bhattacharyya, D.; Tang, K. Adsorptive nanofibrous membranes for bidirectional removal of cationic and anionic dyes. *Sep. Purif. Technol.* **2025**, *361*, 131515. [CrossRef]
19. Sharma, R.; Kumar, N.; Sharma, P.; Yadav, A.; Aggarwal, N.K. Biological decolorisation of the anionic Dye Acid Blue 9 by bacterial consortium: A sustainable and ecofriendly approach for the treatment of textile wastewater. *Sustain. Chem. Environ.* **2024**, *8*, 100178. [CrossRef]
20. Tajat, N.; El Hayaoui, W.; El Mouhri, W.; Bougdour, N.; Idlahcen, A.; Radaa, C.; Bakas, I.; Tamimi, M.; Badreddine, M.; Assabbane, A.; et al. Simultaneous removal of anionic and cationic dyes from aqueous solutions using nickel–iron layered double hydroxide nanosheets. *Int. J. Environ. Sci. Technol.* **2024**, *21*, 2843–2862. [CrossRef]
21. Abid, M.F.; Zablouk, M.A.; Abid-Alameer, A.M. Experimental study of dye removal from industrial wastewater by membrane technologies of reverse osmosis and nanofiltration. *Iran. J. Environ. Health Sci. Eng.* **2012**, *9*, 17. [CrossRef] [PubMed]
22. Lashgari, M.; Naseri-Moghanlou, S.; Khanahmadlou, T.; Hempelmann, R. Electrostatic boosting of ionic dye pollutant removal from aquatic environment using a single electrode photoreactor. *NPJ Clean Water* **2023**, *6*, 10. [CrossRef]
23. Khan, S.; Noor, T.; Iqbal, N.; Yaqoob, L. Photocatalytic Dye Degradation from Textile Wastewater: A Review. *ACS Omega* **2024**, *9*, 21751–21767. [CrossRef]
24. Suhas; Kushwaha, S.; Chaudhary, M.; Chaudhary, S.; Tyagi, V.; Cansado, I.P.; Dehghani, M.H. Effect of substituent groups on the adsorption efficiency of phenols by activated carbon developed by hydrothermally treated *Phyllanthus emblica* fruit stone. *Toxics* **2024**, *12*, 874. [CrossRef] [PubMed]
25. Chaudhary, M.; Suhas; Singh, R.; Tyagi, I.; Ahmed, J.; Chaudhary, S.; Kushwaha, S. Microporous activated carbon as adsorbent for the removal of noxious anthraquinone acid dyes: Role of adsorbate functionalization. *J. Environ. Chem. Eng.* **2021**, *9*, 106308. [CrossRef]
26. Dalmaz, A.; Sivrikaya Özak, S. Methylene blue dye efficient removal using activated carbon developed from waste cigarette butts: Adsorption, thermodynamic and kinetics. *Fuel* **2024**, *372*, 132151. [CrossRef]
27. Soualili, A.; Attouti, S.; Termoul, M.; Benzekri-Benallou, M.; Bestani, B.; Benderdouche, N.; Sreńscek-Nazza, J.; Michalkiewicz, B. Wild reed waste as a biosorbent for toxicity lowering of selected pollutants: Isotherms, kinetic and thermodynamic studies. *Desalination Water Treat.* **2024**, *318*, 100348. [CrossRef]
28. Suhas; Kushwaha, S.; Tyagi, I.; Ahmed, J.; Chaudhary, S.; Chaudhary, M.; Stephen Inbaraj, B.; Goscianska, J.; Karri, R.R.; Sridhar, K. Adsorptive Analysis of Azo Dyes on Activated Carbon Prepared from *Phyllanthus emblica* Fruit Stone Sequentially via Hydrothermal Treatment. *Agronomy* **2022**, *12*, 2134. [CrossRef]
29. Suhas; Chaudhary, M.; Chaudhary, S.; Singh, M.; Dehghani, M.H.; Tyagi, I.; Cansado, I.P.P.; Kumar, S.; Kumar, S. An ingenious investigation on the adsorptive and antibacterial properties of a novel silver-doped hydrochar. *Int. J. Environ. Sci. Technol.* **2024**, *21*, 8595–8606. [CrossRef]
30. Kumar, S.; Sharma, S.; Kumar, V.; Sharma, A.; Kaur, R.; Saini, R. Jamun (*Syzygium cumini* (L.) *Skeels*): The conventional underutilized multifunctional plant-an exotic gleam into its food and functional significance. *Ind. Crops Prod.* **2023**, *191*, 115873. [CrossRef]
31. Kaur, I.; Sharma, A.D.; Samtiya, M.; Pereira-Caro, G.; Rodríguez-Solana, R.; Dhewa, T.; Moreno-Rojas, J.M. Potential of bioactive compounds derived from underutilized fruit-bearing plants: A comprehensive review. *Eur. Food Res. Technol.* **2023**, *249*, 553–572. [CrossRef]
32. Eslamipoor, R.; Sepehriar, A. Enhancing supply chain relationships in the circular economy: Strategies for a green centralized supply chain with deteriorating products. *J. Environ. Manag.* **2024**, *367*, 121738. [CrossRef] [PubMed]

33. Fernandez, M.E.; Ledesma, B.; Román, S.; Bonelli, P.R.; Cukierman, A.L. Development and characterization of activated hydrochars from orange peels as potential adsorbents for emerging organic contaminants. *Bioresour. Technol.* **2015**, *183*, 221–228. [CrossRef] [PubMed]
34. *3175-07*; A.S.D. Test Method for Volatile Matter in the Analysis Sample of Coal and Coke. 2011. Available online: https://cdn.standards.iteh.ai/samples/53346/f8058fb13177432e8efc47a1c24017b9/ASTM-D3175-07.pdf (accessed on 27 January 2025).
35. *E1755-01*; Standard Test Method for Ash in Biomass. 2024. Available online: https://www.astm.org/e1755-01r20.html (accessed on 27 January 2025).
36. *4442-07*; A.s.D. Standard Test Methods for Direct Moisture Content Measurement of Wood and Wood-Base Materials. ASTM International, 2007. Available online: https://archive.org/details/gov.law.astm.D4442.07 (accessed on 27 January 2025).
37. Carrott, P.J.M.; Carrott, M.M.L.R.; Vale, T.S.C.; Marques, L.; Nabais, J.M.V.; Mourão, P.A.M.; Suhas, P.A.M. Characterisation of surface ionisation and adsorption of phenol and 4-nitrophenol on non-porous carbon blacks. *Adsorpt. Sci. Technol.* **2008**, *26*, 827–841. [CrossRef]
38. Raspolli Galletti, A.M.; D'Alessio, A.; Licursi, D.; Antonetti, C.; Valentini, G.; Galia, A.; Nassi o Di Nasso, N. Midinfrared FT-IR as a tool for monitoring herbaceous biomass composition and its conversion to furfural. *J. Spectrosc.* **2015**, *2015*, 719042. [CrossRef]
39. Adeniyi, A.G.; Ighalo, J.O.; Onifade, D.V. Production of biochar from elephant grass (*Pernisetum purpureum*) using an updraft biomass gasifier with retort heating. *Biofuels* **2021**, *12*, 1283–1290. [CrossRef]
40. Jiang, Z.; Li, J.; Jiang, D.; Gao, Y.; Chen, Y.; Wang, W.; Cao, B.; Tao, Y.; Wang, L.; Zhang, Y. Removal of atrazine by biochar-supported zero-valent iron catalyzed persulfate oxidation: Reactivity, radical production and transformation pathway. *Environ. Res.* **2020**, *184*, 109260. [CrossRef] [PubMed]
41. Mishra, S.K.; Tripathi, S.N.; Choudhary, V.; Gupta, B.D. Surface plasmon resonance-based fiber optic methane gas sensor utilizing graphene-carbon nanotubes-poly(methyl methacrylate) hybrid nanocomposite. *Plasmonics* **2015**, *10*, 1147–1157. [CrossRef]
42. Pimentel, C.H.; Freire, M.S.; Gómez-Díaz, D.; González-Álvarez, J. Preparation of activated carbon from pine (*Pinus radiata*) sawdust by chemical activation with zinc chloride for wood dye adsorption. *Biomass Convers. Biorefinery* **2023**, *13*, 16537–16555. [CrossRef]
43. Santhosh, A.; Dawn, S.S. Synthesis of zinc chloride activated eco-friendly nano-adsorbent (activated carbon) from food waste for removal of pollutant from biodiesel wash water. *Water Sci. Technol.* **2021**, *84*, 1170–1181. [CrossRef] [PubMed]
44. Rouquerol, J.; Rouquerol, F.; Llewellyn, P.; Maurin, G.; Sing, K. *Adsorption by Powders and Porous Solids: Principles, Methodology and Applications*; Academic Press: Cambridge, MA, USA, 2013.
45. Haghighizadeh, M.; Zare, K.; Aghaie, H.; Monajjemi, M. Preparation and characterization of Chicory leaf powder and its application as a nano-native plant sorbent for removal of Acid Blue 25 from aqueous media: Isotherm, kinetic and thermodynamic study of the adsorption phenomenon. *J. Nanostructure Chem.* **2020**, *10*, 75–86. [CrossRef]
46. Aksu, Z.; Akın, A.B. Comparison of Remazol Black B biosorptive properties of live and treated activated sludge. *Chem. Eng. J.* **2010**, *165*, 184–193. [CrossRef]
47. Cotoruelo, L.M.; Marqués, M.D.; Díaz, F.J.; Rodríguez-Mirasol, J.; Rodríguez, J.J.; Cordero, T. Lignin-based activated carbons as adsorbents for crystal violet removal from aqueous solutions. *Environ. Prog. Sustain. Energy* **2012**, *31*, 386–396. [CrossRef]
48. Aumeier, B.M.; Augustin, A.; Thönes, M.; Sablotny, J.; Wintgens, T.; Wessling, M. Linking the effect of temperature on adsorption from aqueous solution with solute dissociation. *J. Hazard. Mater.* **2022**, *429*, 128291. [CrossRef]
49. Esvandi, Z.; Foroutan, R.; Peighambardoust, S.J.; Akbari, A.; Ramavandi, B. Uptake of anionic and cationic dyes from water using natural clay and clay/starch/MnFe2O4 magnetic nanocomposite. *Surf. Interfaces* **2020**, *21*, 100754. [CrossRef]
50. Cruz Jr, O.F.; Serafin, J.; Azar, F.-Z.; Casco, M.E.; Silvestre-Albero, J.; Hotza, D.; Rambo, C.R. Microwave-Assisted hydrothermal carbonization and characterization of Amazonian biomass as an activated carbon for methane adsorption. *Fuel* **2024**, *358*, 130329. [CrossRef]
51. Xu, J.; Wang, L.; Zhu, Y. Decontamination of Bisphenol A from aqueous solution by graphene adsorption. *Langmuir* **2012**, *28*, 8418–8425. [CrossRef]
52. Baccar, R.; Blánquez, P.; Bouzid, J.; Feki, M.; Sarrà, M. Equilibrium, thermodynamic and kinetic studies on adsorption of commercial dye by activated carbon derived from olive-waste cakes. *Chem. Eng. J.* **2010**, *165*, 457–464. [CrossRef]
53. Jaguaribe, E.; Medeiros, L.; Barreto, M.; Araujo, A. The performance of activated carbons from sugarcane bagasse, babassu, and coconut shells in removing residual chlorine. *Braz. J. Chem. Eng.* **2005**, *22*, 41–47. [CrossRef]
54. Shabir, S.; Hussain, S.Z.; Bhat, T.A.; Amin, T.; Beigh, M.; Nabi, S. High carbon content microporous activated carbon from thin walnut shells: Optimization, physico-chemical analysis and structural profiling. *Process Saf. Environ. Prot.* **2024**, *190*, 85–96. [CrossRef]
55. Langmuir, I. The adsorption of gases on plane surfaces of glass, mica and platinum. *J. Am. Chem. Soc.* **1918**, *40*, 1361–1403. [CrossRef]
56. Freundlich, H. Over the adsorption in solution. *J. Phys. Chem.* **1906**, *57*, 1100–1107.
57. Temkin, M. Kinetics of ammonia synthesis on promoted iron catalysts. *Acta Physiochim. URSS* **1940**, *12*, 327–356.

58. Dubinin, M. The equation of the characteristic curve of activated charcoal. In Proceedings of the Doklady Akademii Nauk SSSR (DAN SSSR), USSR; 1947; pp. 327–329. Available online: https://www.scirp.org/reference/referencespapers?referenceid=1215724 (accessed on 27 January 2025).
59. Lagergren, S.K. About the theory of so-called adsorption of soluble substances. *Sven. Vetenskapsakad. Handingarl* **1898**, *24*, 1–39.
60. Ho, Y.S.; McKay, G. Sorption of dye from aqueous solution by peat. *Chem. Eng. J.* **1998**, *70*, 115–124. [CrossRef]
61. Elovich, S.J. Proceedings of the Second International Congress on Surface Activity. Schulman, J.H., Ed.; Academic Press, Inc: New York, NY, USA, 1959; Volume 11, p. 253.
62. Weber, W.; Morris, J. Advances in water pollution research. In Proceedings of the First International Conference on Water Pollution Research; 1962; p. 231.
63. Atkins, P.; Atkins, P.W.; de Paula, J. *Atkins' Physical Chemistry*; Oxford University Press: Oxford, UK, 2014.
64. Islam, M.A.; Benhouria, A.; Asif, M.; Hameed, B.H. Methylene blue adsorption on factory-rejected tea activated carbon prepared by conjunction of hydrothermal carbonization and sodium hydroxide activation processes. *J. Taiwan. Inst. Chem. Eng.* **2015**, *52*, 57–64. [CrossRef]
65. Hammud, H.H.; Shmait, A.; Hourani, N. Removal of Malachite Green from water using hydrothermally carbonized pine needles. *RSC Adv.* **2015**, *5*, 7909–7920. [CrossRef]
66. Genli, N.; Kutluay, S.; Baytar, O.; Şahin, Ö. Preparation and characterization of activated carbon from hydrochar by hydrothermal carbonization of chickpea stem: An application in methylene blue removal by RSM optimization. *Int. J. Phytoremediation* **2022**, *24*, 88–100. [CrossRef] [PubMed]
67. da Silva Lacerda, V.; López-Sotelo, J.B.; Correa-Guimarães, A.; Hernández-Navarro, S.; Sánchez-Báscones, M.; Navas-Gracia, L.M.; Martín-Ramos, P.; Martín-Gil, J. Rhodamine B removal with activated carbons obtained from lignocellulosic waste. *J. Environ. Manag.* **2015**, *155*, 67–76. [CrossRef]